THE JOURNAL OF PHYSICAL CHEMISTRY B LETTERS

2005, *109,* 18218−18222
Published on Web 09/13/2005

Cu Nanoshells: Effects of Interband Transitions on the Nanoparticle Plasmon Resonance

Hui Wang,[†,‡] Felicia Tam,[‡,§] Nathaniel K. Grady,[‡,||] and Naomi J. Halas*[,†,‡,||]

Department of Chemistry, Department of Physics and Astronomy, Department of Electrical and Computer Engineering, and the Laboratory for Nanophotonics, Rice University, Houston, Texas 77005

Received: July 13, 2005; In Final Form: August 22, 2005

The optical properties of metals arise both from optical excitation of interband transitions and their collective electronic, or plasmon, response. Here, we examine the optical properties of Cu, whose strong interband transitions dominate its optical response in the visible region of the spectrum, in a nanoshell geometry. This nanostructure permits the geometrical tuning of the nanoparticle plasmon energy relative to the onset of interband transitions in the metal. Spectral overlap of the interband transitions of Cu with the nanoshell plasmon resonance results in a striking double-peaked plasmon resonance, a unique phenomenon previously unobserved in other noble or coinage metal nanostructures.

Metallic nanostructures are attracting increasing interest as an important class of photonic components that control and manipulate light at the nanometer scale.[1−4] The interaction of light with free electrons in metallic nanostructures can give rise to collective excitations known as plasmon resonances. Plasmonic excitations provide a means to focus light to subwavelength dimensions, making it possible to overcome the optical diffraction limit and enable the design of nanoscale optical devices, such as waveguides.[3,5] The intense local electromagnetic fields of metallic nanostructures at their plasmon resonant energies can also be exploited for surface enhanced spectroscopies.[6−8] Recent advances in size- and shape-controlled fabrication of metallic nanostructures,[9] along with the development of highly efficient theoretical methods for calculating their electromagnetic properties,[10−12] provide a foundation for advancing the development of metal-based nanophotonic components and devices, an emerging area known as plasmonics.

Coinage metals such as Au and Ag have been of particular interest for plasmonics because they can support nanoparticle plasmon resonances in the ultraviolet, visible, and near-infrared regions of the spectrum, modifiable by varying nanoparticle size and shape. Metallic nanoshells, spherical nanoparticles composed of a dielectric core and a concentric metal shell, are nanoparticles whose plasmon resonant energies are particularly sensitive to geometry.[13] In striking contrast to solid metallic nanostructures such as nanospheres or nanorods, which exhibit relatively weak plasmonic tunability dependent on size or aspect ratio, nanoshells exhibit plasmon resonances that are critically dependent on inner and outer shell dimensions. This tunability has its origins in the hybridization of the two fixed-frequency plasmon modes supported by the inner cavity and outer surface of the nanoshell.[14] In applications, plasmon resonant energies of nanoshells have been tuned to the near-infrared "water window" where tissue and blood are transparent, enabling a range of nanobiomedical innovations.[15−18] The plasmon resonant energy of the nanoshell geometry can be extended into the far-infrared through plasmon hybridization of one nanoshell encapsulated within another nanoshell, also known as a "nanomatryushka" geometry.[14,19] Because of their high degree of symmetry, many nanoshell properties can be calculated straightforwardly using Mie scattering theory.[20,21] The agreement between experimental measurements and Mie theory predictions of the plasmon resonant properties of Au nanoshells has recently been further confirmed quantitatively at the single nanoparticle level.[22]

In addition to nanoparticle geometry, the optical properties of plasmonic nanoparticles can also be strongly influenced by the electronic structure of the constituent metal, which determines the metal's dielectric function.[23,24] To better understand the role that the metal plays in determining the optical properties of metallic nanoparticles, it is necessary to examine and account for the effects of both the free-electron and electronic interband transition contributions to the metal's dielectric response.[25] With plasmon resonant energies well below the interband transitions, Au and Ag nanoparticles can be treated as free-electron systems whose optical properties are determined by the conduction electrons, with only a constant real background polarizability associated with the core electrons. Here, we both theoretically and experimentally examine the contrasting case of Cu nanoparticles, where the effects of strong interband transitions near the same energies as the plasmon response of the solid metallic nanoparticle can be examined. Geometric control of the plasmon resonant energies in the nanoshell geometry enables selective tuning of plasmon mode energies with respect to the onset of the Cu interband transitions. By varying nanoparticle geometry, we examine how the electronic properties of the metal, through the interband transitions, modify the plasmon resonances of the constituent nanoparticle.

* To whom correspondence should be addressed. E-mail: halas@rice.edu. Phone: 1-(713) 348-5611. Fax: 1-(713) 348-5686.
[†] Department of Chemistry.
[‡] The Laboratory for Nanophotonics.
[§] Department of Physics and Astronomy.
[||] Department of Electrical and Computer Engineering.

10.1021/jp053863t CCC: $30.25

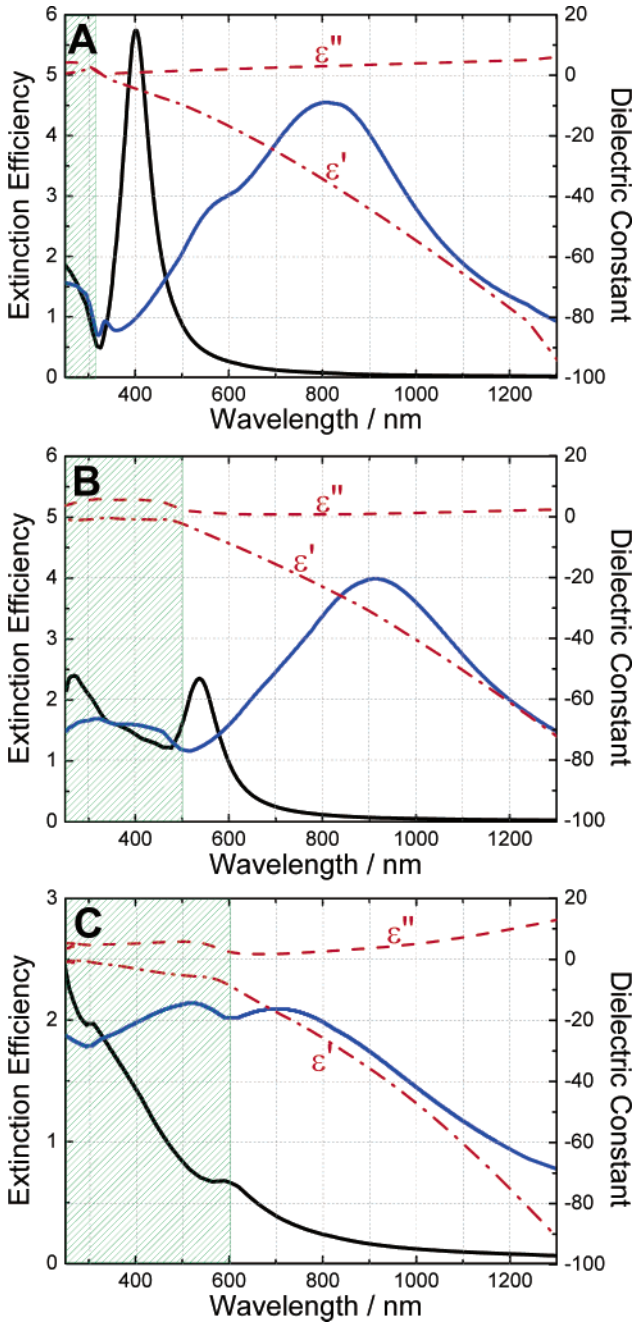

Figure 1. Theoretically calculated far-field extinction of a solid nanosphere (black solid curves) and a nanoshell (blue solid curves) made of (A) Ag, (B) Au, and (C) Cu. The nanospheres are 20 nm in radius, and the nanoshells are 63 nm in core (silica) radius and 10 nm in shell thickness. The refractive index of ethanol ($n = 1.36$) is used as the refractive index of the medium surrounding the particles. The dielectric functions (red curves) of (A) Ag, (B) Au, and (C) Cu are also shown. ϵ' and ϵ'' are the real and imaginary parts of the dielectric constants, respectively. The green shaded areas indicate the wavelength regions where interband transitions of the metals occur.

Figure 1 shows a comparison of the theoretical extinction spectra of Au, Ag, and Cu solid nanospheres and nanoshells, obtained using Mie scattering theory incorporating the experimentally obtained dielectric function for Ag, Au, and Cu[26] and standard finite path length corrections.[23,27] The surrounding dielectric medium is ethanol (refractive index 1.36). The calculated extinction is expressed as an efficiency, which is the ratio of the energy scattered or absorbed by the nanoparticle to the energy incident on its physical cross section. The spectral regions where interband transitions occur are shaded in green.

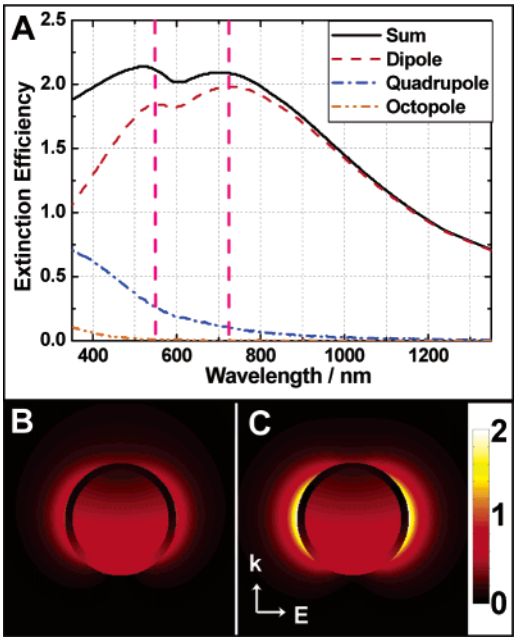

Figure 2. (A) Theoretically calculated far-field extinction of a Cu nanoshell with a core radius of 63 nm and a shell thickness of 10 nm. Near-field patterns of the dipole resonance excited at (B) 550 nm and (C) 720 nm. The polarization (E) and propagation (k) vectors are indicated in part C. The color scale indicates $|E|^2$.

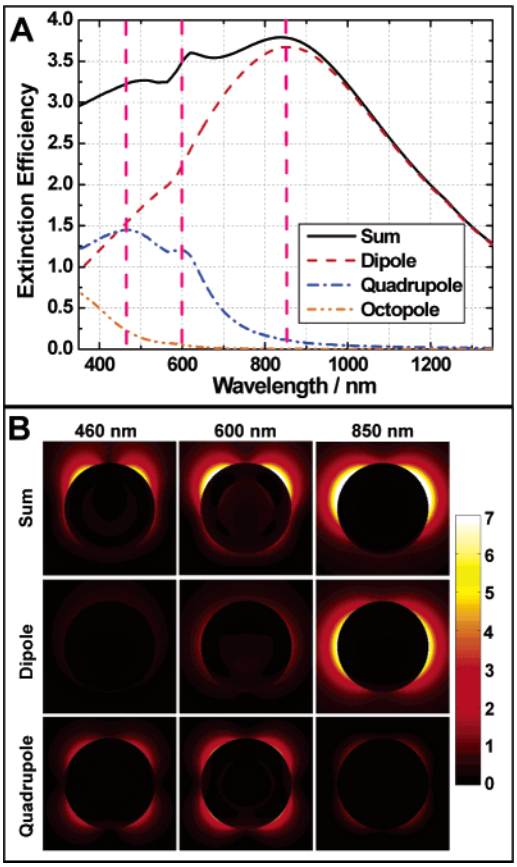

Figure 3. (A) Theoretically calculated far-field extinction of a Cu nanoshell with a core radius of 63 nm and a shell thickness of 40 nm. (B) Near-field pattern in the plane containing the polarization and propagation vectors as indicated in Figure 2. The color bars indicate the magnitude of $|E|^2$. The columns indicate the excitation wavelengths. The first row includes the first five terms in the Mie expansion, the second row contains only the first (dipole) term, and the third row includes only the second (quadrupole) term.

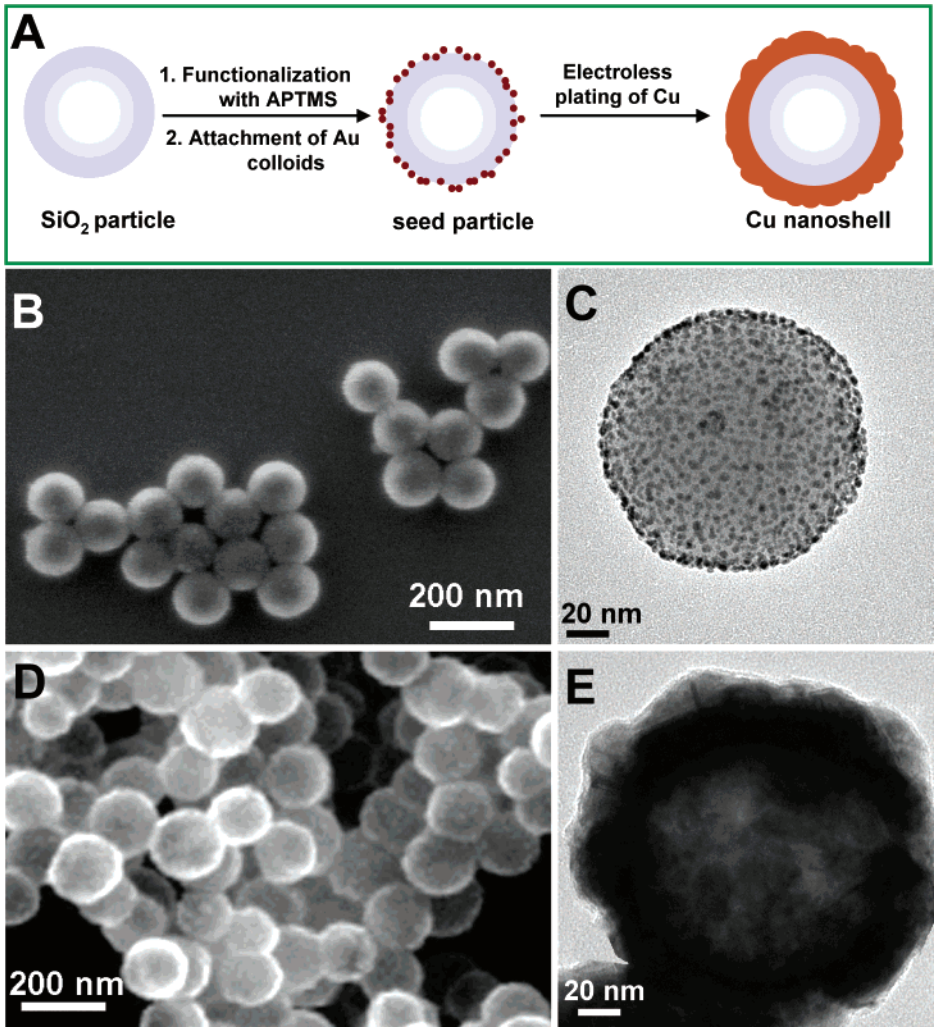

Figure 4. (A) Illustration of the fabrication of Cu nanoshells. SEM (B) and TEM (C) images of the seed particles. SEM (D) and TEM (E) images of Cu nanoshells (63 ± 8 nm core radius and 30 ± 4 nm shell thickness).

The onset of electronic interband transitions from the valence band to the Fermi level causes a sharp increase in the imaginary part (ϵ'') and a marked change in the slope of the real part (ϵ') of the dielectric functions. For 20 nm radius solid nanospheres, the relative spectral locations of the particle plasmon resonance and the constituent metal's interband transitions determine the nanoparticles' optical response, resulting in significant variations between Au, Ag, and Cu nanospheres. The Ag nanosphere has by far the strongest plasmon resonance because the higher energy of the interband transitions (~3.8 eV),[28,29] relative to the energy of the plasmon resonance, leads to minimal damping of the plasmon. In Ag, the onset of interband transitions is visible in the experimental extinction spectrum only as a small increase in absorption starting at approximately 330 nm. The Au nanosphere displays a well-defined plasmon resonance at 530 nm, which is very close to the edge of the interband transitions region (~2.5 eV).[28,29] The Cu nanosphere has by far the weakest comparative optical response due to the nanosphere plasmon being resonant with the interband transition region (~2.1 eV)[28−30] of the spectrum. The interband transitions are responsible for a strong damping of the Cu nanosphere plasmon and the strong "background" absorption on top of which a weak plasmon resonance peak is visible.

The tunability of nanoshell plasmons allows the design of nanoparticles with surface plasmon resonances shifted away from the constituent metal's interband transitions. A direct comparison of theoretical extinction spectra for nanoshells composed of a silica core and Ag, Au, and Cu shell layers is also shown in Figure 1. All nanoshell calculations were performed with the same inner and outer shell radii (r_1, r_2) = (63, 73) nm. All nanoshell spectra exhibit dipole plasmon resonances that have been shifted to longer wavelengths relative to those of the corresponding solid nanospheres. The plasmon resonance spectra of the Ag and Au nanoshells in parts A and B of Figure 1, respectively, are relatively similar to each other in amplitude and peak wavelength, a comparison that has been previously noted.[31] The Ag nanoshell resonance also shows an additional, weaker feature at nominally 560 nm attributable to excitation of the nanostructure's quadrupole mode. In marked contrast, the plasmon resonance of a Cu nanoshell of the same size and aspect ratio remains centered at wavelengths corresponding to the onset of interband transitions in Cu (Figure 1C). In addition, a dip in the resonance spectrum also appears at this onset energy, resulting in a unique double-peaked resonance line shape.

In Figure 2, the Cu nanoshell resonance line shape is analyzed in greater detail. In Figure 2A, the total calculated far-field extinction spectrum is analyzed to show the individual dipole, quadrupole, and octopole contributions to the overall spectral response of the nanostructure. The overall extinction is dominated by the dipole plasmon mode, whose line shape has been strongly modified into this double-peaked structure. This analysis clearly shows that the origin of this double-peaked feature is related to variations in the dielectric function of Cu,

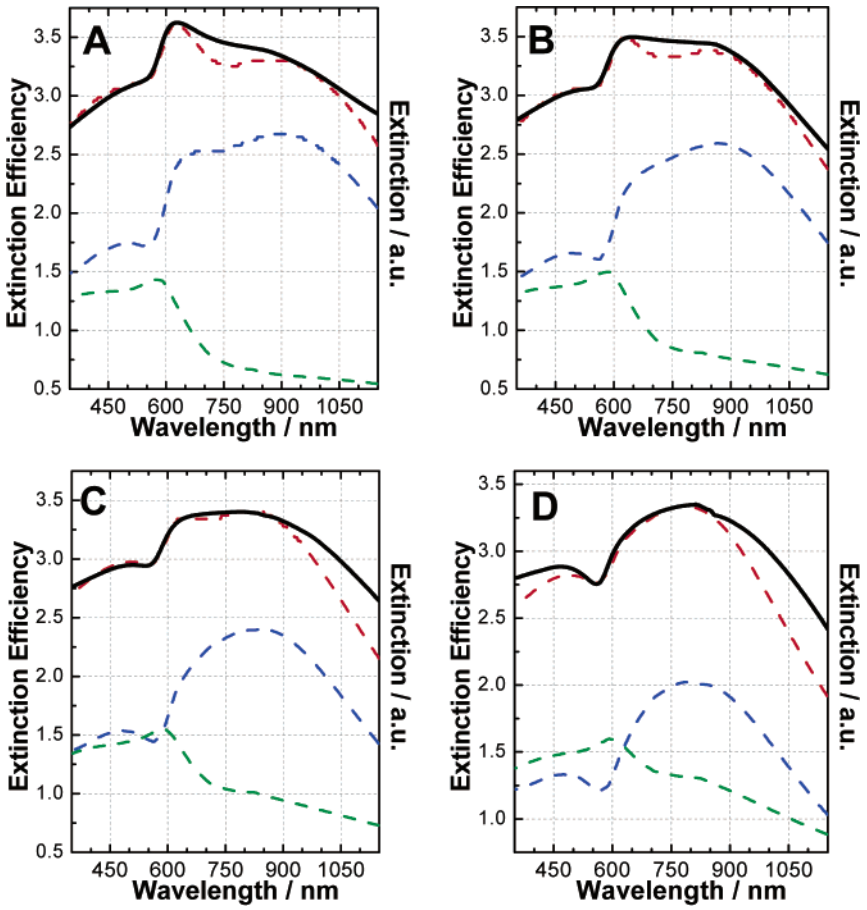

Figure 5. Extinction spectra of Cu nanoshells with a core radius of 63 ± 8 nm and a shell thickness of (A) 52 ± 7 nm, (B) 45 ± 6 nm, (C) 38 ± 5 nm, and (D) 30 ± 4 nm. The solid curves are the experimentally measured extinction spectra of Cu nanoshells dispersed in ethanol. The dashed curves are the theoretically calculated extinction (red), absorption (green), and scattering (blue) of the Cu nanoshells.

and not due to the onset of a quadrupole mode (such as the high energy feature at ~550 nm in the Ag nanoshell response in Figure 1A). As illustrated in Figure 2B and C, the near-field contours of the plasmon resonance excited at 550 and 720 nm, wavelengths corresponding to the two maxima of this resonance, further confirm the dipolar nature of each spectral feature. As the thickness of the Cu nanoshell layer is increased, the quadrupole plasmon mode can be brought into resonance with the interband transitions in Cu. The peak of the dipole resonance is shifted to ~ 850 nm, and the quadrupole and other higher order multiple modes become increasingly pronounced compared to the dipole resonance, due to increasing phase retardation effects.[32−34] In this case, the peculiar peak "inflection" is transferred to the quadrupole plasmon mode (Figure 3A). Figure 3A analyzes the calculated extinction spectrum of a (63, 103) Cu nanoshell. Here, both the dipole and quadrupole modes contribute significantly to the overall extinction. A double-peaked quadrupole line shape is now observed as the quadrupole resonance overlaps with the onset of the interband transitions. The quadrupole maximum at 460 nm is more intense than that at 600 nm and is likely due to the overlap of the quadrupole plasmon resonance with the spectral background arising from the interband transitions. Figure 3B shows the calculated near-field contours of the dipole and quadrupole plasmon modes excited at the wavelengths associated with these inflections, as indicated in Figure 3A. The top row in Figure 3B corresponds to the total plasmon extinction in the near-field at these three wavelengths of interest, which in this case consists of the sum of the first five multipolar terms in the Mie expansion. The asymmetry of the total near-field profile is simply due to the relative phase of the various multipolar modes. The second row shows the relative dipole mode intensities in the near-field at the three wavelengths of interest, and the third row shows the quadrupole mode. The near-field patterns confirm the quadrupolar nature of both spectral features at 460 and 600 nm for this size and geometry of nanoparticle.

To experimentally investigate the effects of interband transitions on the plasmons, we use a wet chemistry method to fabricate Cu nanoshells with controllable core−shell dimensions. Currently, the most extensively used strategy for nanoshell fabrication involves seed-mediated electroless plating. By using this method, continuous Au,[13,35−37] Ag,[31,38,39] and even bimetallic nanoshells[40] with controllable core and shell dimensions have been successfully fabricated using silica or polymer beads as core materials. In addition to the seeded shell growth, more recent approaches based on galvanic replacement reactions[41−43] have also been employed to produce hollow metallic nanoshells using metal nanoparticles as sacrificial cores. Here, we exploit a combination of surface seeding and electroless plating methods to fabricate Cu nanoshells using silica nanosphere cores (Figure 4). As illustrated in Figure 4A, the fabrication of Cu nanoshells involves two major steps. The first step is analogous to the pretreatment step in electroless plating, in which small Au nanoparticles (~2 nm in diameter) are immobilized onto the surface of (3-aminopropyl)trimethoxysilane (APTMS) functionalized silica particles. As illustrated in Figure 4C, the coverage of Au nanoparticles on the surface of the silica beads is nominally 30%. In the second step, the immobilized Au colloids act as nucleation sites for electroless Cu plating onto the surface of silica particles, leading to the gradual formation

of continuous and complete Cu nanoshells (Figure 4D and F). The as-prepared Cu nanoshells can be homogeneously dispersed in ethanol to form colloidal solutions. X-ray powder diffraction results (Supporting Information) indicate the absence of oxide layers on the surface of the as-prepared Cu nanoshells during and after the shell growth.

Figure 5 shows the extinction spectra of experimentally fabricated Cu nanoshells with a core radius of 63 ± 8 nm and several varying shell thicknesses. The core and shell dimensions of the Cu nanoshells are determined according to scanning electron microscopy (SEM) images obtained of the nanostructures. The standard deviations of the core size and shell thickness are also included for the theoretical calculations. The experimental plasmon response is in each case compared with the response obtained using Mie scattering theory, and the relative contributions of absorption and scattering to the overall extinction spectra of the nanoparticles are shown. The positions and line shapes of the plasmon peaks in the measured extinction spectra are in good agreement with Mie scattering theory. Three discernible peaks are observed. The peak in the range 800−900 nm is identified as the dipole resonance, and the peak inflections observed at ∼620 and ∼470 nm correspond quite well to the predicted peak splitting discussed earlier (Figures 2 and 3). As the shell thickness increases, the quadrupole resonance becomes increasingly pronounced compared to the dipole resonance, and the dipole peak red-shifts only slightly. These effects are due to phase retardation which increases with the particle size.[34]

In conclusion, the effects of interband transitions on the optical properties of metallic nanoparticles have been observed and investigated in the Cu nanoshell geometry. When a dipole or quadrupole plasmon overlaps the interband transition threshold, a double-peaked plasmon resonance appears. The measured extinction spectra of experimentally fabricated Cu nanoshells are in good agreement with Mie scattering theory and exhibit this behavior for a variety of shell thicknesses. In photonic device applications, Cu may potentially be desirable over Au or Ag due to its compatibility with Si-based processing. Cu nanoshells are of significant interest for potential large-scale or large-area applications relative to their Au and Ag counterparts due to the significantly reduced relative cost of the constituent metal. In a more general sense, developing a better understanding of the role of electronic structure in the optical properties of metallic nanostructures may lead to increased interest in the development of plasmonic nanostructures based on other material systems, incorporating additional properties and functionalities.

Acknowledgment. We gratefully acknowledge the National Science Foundation (NSF) grant EEC-0304097, Air Force Office of Scientific Research grant F49620-03-C-0068, the Texas Institute for Bio-Nano Materials and Structures for Aerospace Vehicles funded by NASA Cooperative Agreement No. NCC-1-02038, Robert A. Welch Foundation grants C-1220, and Multidisciplinary University Research Initiative (MURI) grant W911NF-04-01-0203 for their financial support.

Supporting Information Available: Experimental details on the fabrication of Cu nanoshells and X-ray powder diffraction results. This material is available free of charge via the Internet at http://pubs.acs.org.

References and Notes

(1) Ebbesen, T. W.; Lezec, H. J.; Ghaemi, H. F.; Thio, T.; Wolff, P. A. *Nature* **1998**, *391*, 667.

(2) Pendry, J. B. *Phys. Rev. Lett.* **2000**, *85*, 3966.

(3) Maier, S. A.; Brongersma, M. L.; Kik, P. G.; Meltzer, S.; Requicha, A. A. G.; Atwater, H. A. *Adv. Mater.* **2001**, *13*, 1501.

(4) Maier, S. A.; Kik, P. G.; Atwater, H. A.; Meltzer, S.; Harel, E.; Koel, B. E.; Requicha, A. A. G. *Nat. Mater.* **2003**, *2*, 229.

(5) Barnes, W. L.; Dereux, A.; Ebbesen, T. W. *Nature* **2003**, *424*, 824.

(6) Nie, S.; Emory, S. R. *Science* **1997**, *275*, 1102.

(7) Kneipp, K.; Wang, Y.; Kneipp, H.; Perelman, L. T.; Itzkan, I.; Dasari, R. R.; Feld, M. S. *Phys. Rev. Lett.* **1997**, *78*, 1667.

(8) Jackson, J. B.; Halas, N. J. *Proc. Natl. Acad. Sci. U.S.A.* **2004**, *101*, 17930.

(9) Xia, Y., Halas, N., Eds. *MRS Bull.* **2005**, *30* (5) (an issue on "Shape-Controlled Synthesis and Suface Plasmonic Properties of Metallic Nanostructures").

(10) Kelly, K. L.; Coronado, E.; Zhao, L. L.; Schatz, G. C. *J. Phys. Chem. B* **2003**, *107*, 668.

(11) Maier, S. A.; Kik, P. G.; Atwater, H. A. *Phys. Rev. B* **2003**, *67*, Art. No. 205402.

(12) Oubre, C.; Nordlander, P. *J. Phys. Chem. B* **2004**, *108*, 17740.

(13) Oldenburg, S. J.; Averitt, R. D.; Westcott, S. L.; Halas, N. J. *Chem. Phys. Lett.* **1998**, *288*, 243.

(14) Prodan, E.; Radloff, C.; Halas, N. J.; Nordlander, P. *Science* **2003**, *302*, 419.

(15) Sershen, S. R.; Westcott, S. L.; Halas, N. J.; West, J. L. *J. Biomed. Mater. Res.* **2000**, *51*, 293.

(16) Loo, C.; Lowery, A.; Halas, N.; West, J.; Drezek, R. *Nano Lett.* **2005**, *5*, 709.

(17) Loo, C.; Lin, A.; Hirsch, L.; Lee, M. H.; Barton, J.; Halas, N.; West, J.; Drezek, R. *Technol. Cancer Res. Treat.* **2004**, *3*, 33.

(18) Hirsch, L. R.; Stafford, R. J.; Bankson, J. A.; Sershen, S. R.; Rivera, B.; Price, R. E.; Hazle, J. D.; Halas, N. J.; West, J. L. *Proc. Natl. Acad. Sci. U.S.A.* **2003**, *100*, 13549.

(19) Radloff, C.; Halas, N. J. *Nano Lett.* **2004**, *4*, 1323.

(20) Aden, A. L.; Kerker, M. *J. Appl. Phys.* **1951**, *22*, 1242.

(21) Neeves, A. E.; Birnboim, M. H. *J. Opt. Soc. Am. B* **1989**, *6*, 787.

(22) Nehl, C.; Grady, N.; Goodrich, G. P.; Tam, F.; Halas, N. J.; Hafner, J. *Nano Lett.* **2004**, *4*, 2355.

(23) Kreibig, U.; Vollmer, M. *Optical Properties of Metal Clusters*; Springer-Verlag: Berlin, Germany, 1995.

(24) Grady, N. K.; Halas, N. J.; Nordlander, P. *Chem. Phys. Lett.* **2004**, *399*, 167.

(25) Marton, J. P.; Jordan, B. D. *Phys. Rev. B* **1977**, *15*, 1719.

(26) *CRC Handbook of Chemistry and Physics*; Lide, D. R., Ed.; CRC Press: Boca Raton, FL, 2000.

(27) Wiesner, J.; Wokaun, A. *Chem. Phys. Lett.* **1989**, *157*, 569.

(28) Johnson, P. B.; Christy, R. W. *Phys. Rev. B* **1972**, *6*, 4370.

(29) Johnson, P. B.; Christy, R. W. *Phys. Rev. B* **1975**, *11*, 1315.

(30) Pinchuk, A.; Kreibig, U.; Hilger, A. *Surf. Sci.* **2004**, *557*, 269.

(31) Jackson, J. B.; Halas, N. J. *J. Phys. Chem. B* **2001**, *105*, 2743.

(32) Oldenburg, S. J.; Jackson, J. B.; Westcott, S. L.; Halas, N. J. *Appl. Phys. Lett.* **1999**, *75*, 2897.

(33) Oldenburg, S. J.; Hale, G. D.; Jackson, J. B.; Halas, N. J. *Appl. Phys. Lett.* **1999**, *75*, 1063.

(34) Westcott, S. L.; Jackson, J. B.; Radloff, C.; Halas, N. J. *Phys. Rev. B* **2002**, *66*, Article No. 155431.

(35) Graf, C.; van Blaaderen, A. *Langmuir* **2002**, *18*, 524.

(36) Lim, Y. T.; Park, O. O.; Jung, H. T. *J. Colloid Interface Sci.* **2003**, *263*, 449.

(37) Shi, W. L.; Sahoo, Y.; Swihart, M. T.; Prasad, P. N. *Langmuir* **2005**, *21*, 1610.

(38) Jiang, Z. J.; Liu, C. Y. *J. Phys. Chem. B* **2003**, *107*, 12411.

(39) Lu, L.; Zhang, H.; Sun, G.; Xi, S.; Wang, H.; Li, X.; Wang, X.; Zhao, B. *Langmuir* **2003**, *19*, 9490.

(40) Liu, J. B.; Dong, W.; Zhan, P.; Wang, S. Z.; Zhang, J. H.; Wang, Z. L. *Langmuir* **2005**, *21*, 1683.

(41) Sun, Y.; Xia, Y. *Anal. Chem.* **2002**, *74*, 5297.

(42) Sun, Y.; Xia, Y. *Nano Lett.* **2003**, *3*, 1569.

(43) Liang, H. P.; Wan, L. J.; Bai, C. L.; Jiang, L. *J. Phys. Chem. B* **2005**, *109*, 7795.